A chromosome-scale genome assembly of Rauvolfia tetraphylla facilitates the identification of the complete ajmaline biosynthetic pathway

Enzo LEZIN[1*], Inês CARQUEIJEIRO[1*], Clément CUELLO[1*], Mickael DURAND[1*], Hans J. JANSEN[2], Valentin VERGÈS[1], Caroline BIRER WILLIAMS[1], Audrey OUDIN[1], Thomas DUGE DE BERNONVILLE[1,‡], Julien PETRIGNET[3], Noémie CELTON[4], Benoit ST-PIERRE[1], Nicolas PAPON[5], Chao SUN[5], Ron P. DIRKS[2], Sarah Ellen O'CONNOR[6,] Michael Krogh JENSEN[7], Sébastien BESSEAU[1,#], Vincent COURDAVAULT[1,#]

[1] Biomolécules et Biotechnologies Végétales, EA2106, Université de Tours, 37200 Tours, France

[2] Future Genomics Technologies, 2333 BE Leiden, The Netherlands

[3] Laboratoire Synthèse et Isolement de Molécules BioActives (SIMBA, EA 7502), Université de Tours, 37200 Tours, France.

[4] Laboratoire de Cytogénetique Constitutionnelle, CHRU de Tours - Hôpital Bretonneau, 37044 Tours, France

[5] Univ Angers, Univ Brest, IRF, SFR ICAT, F-49000 Angers, France

[5] Institute of Medicinal Plant Development, Chinese Academy of Medical Sciences and Peking Union Medical College, Beijing, China

[6] Department of Natural Product Biosynthesis, Max Planck Institute for Chemical Ecology, Jena 07745, Germany

[7] Novo Nordisk Foundation Center for Biosustainability, Technical University of Denmark, Kgs Lyngby, Denmark

*Equal contribution

[‡]Present address: Limagrain, Centre de Recherche, Route d'Ennezat, Chappes, France

[#]**Corresponding authors:** sebastien.besseau@univ-tours.fr (Sébastien Besseau); vincent.courdavault@univ-tours.fr (Vincent Courdavault)

Dear Editor,

Rauvolfia tetraphylla (*aka* the devil-pepper) (**Supplementary Figure S1**) is a well-known medicinal plant producing monoterpenoid indole alkaloids (MIAs). This biosynthesis of MIAs is distributed in several organs including leaves, stems, fruit and roots which accumulates the famous antiarrhythmic ajmaline (Kumar et al. 2016a; Kumar et al., 2016b; Kumara et al. 2019). MIAs are natural products notably involved in plant adaptation to environment and defense against aggressors. This mainly results from their high biological activities that also explain their pharmacological properties. MIAs display complex structures resulting from long and elaborated biogenesis processes as mainly illustrated in the Madagascar periwinkle *Catharanthus roseus* (**Kulagina et al., 2022**). While ajmaline remains an important drug on the general pharmaceutical market, its biosynthetic pathway is still incomplete, thus precluding a transfer in heterologous organisms as recently achieved for the bioproduction of other valuable MIAs (**Zhang et al., 2022**). Overall, the biosynthesis of ajmaline requires a 10-step modification of strictosidine, catalyzed by enzymes from the cytochrome P450, alcohol dehydrogenase (ADH) or BAHD acyltransferase families, which have been all identified but one (**Dang et al., 2017**) (**Supplementary Figure S2**). The central part of this pathway indeed involves the conversion of vinorine into 17-*O*-acetyl-norajmaline. This first relies on the hydroxylation of vinorine into vomilenine by vinorine hydroxylase (VH) (**Dang et al., 2017**). Next, two ADHs successively ensure the reduction of the vomilenine 19,20-double bond and reduction of its indolenine ring in 1,2-position. So far, only the vomilenine reductase (from the medium chain dehydrogenase/reductase family) producing the 19,20-α(S)-dihydrovomilenine has been characterized and named VR2 (Vomilenine Reductase 2, **Geissler et al., 2016**). This thus makes the remaining ADH the only missing enzyme from the ajmaline biosynthetic route.

In order to identify this enzyme, we have first assembled a chromosome-scale version of the *R. tetraphylla* genome by generating 43.8 Gb ONT PromethION reads with an N50 of ~21.8 kb. Reads were assembled with Flye and the resulting contigs were twice corrected with ONT reads and twice polished with Illumina reads. Using Hi-C data (**Supplementary Figure S3A**), 89.7% of the unscaffolded assembly have been anchored to 33 pseudo-chromosomes (**Figure 1A**; **Supplementary Methods**) in accordance with the 66 chromosomes counted in *R. tetraphylla* cells (2n=66, **Supplementary Figure S2B**) resulting in a ~733.6 Mb assembly. About 98.3% of Eudicots Benchmarking Universal Single Copy Orthologs (BUSCO) were annotated and LTR Assembly Index (19.21) was higher than *C. roseus* (13.11 (**Li et al, 2023**) – 14.62 (**Sun et al, 2023**)), indicating the high completeness of our assembly in both genic and non-genic regions (**Supplementary Tables S1**). By integrating *ab initio* prediction and *de novo* transcriptome assembly, we annotated 101,883 high-confidence genes (**Figure 1A**, **Supplementary Tables S1-S2**) with a BUSCO complete score of 97.7%. Functional

annotations could assign ~65.7% of the genes (**Supplementary Table S2**). Transposable elements annotation revealed that ~39% of the genome consists of transposable elements (**Figure 1A, Supplementary Table S3**). An evolutionary analysis indicated that *R. tetraphylla* experienced whole-genome triplication (WGT) which probably resulted from a double hybridization (2n=6x=66, **Figure 1A and B**) and a great expansion of several orthogroups (**Figure 1C; Supplementary Figure S4**). This also resulted in a great expansion of genes encoding ADHs notably including 372 MDRs (medium chain dehydrogenase/reductase), 317 short-chain alcohol dehydrogenases and 135 aldo-keto reductases (**Supplementary Table S4**).

Based on this new genome, we searched for putative natural product biosynthetic gene clusters (**Supplementary Methods**, **Supplementary Tables S5-6**). Among them, we identified 3 genomic regions located on the chromosomes 11a, 11b and 11c, which respectively consist in 10, 9 and 9 successive genes encoding ADHs that all correspond to cinnamyl-alcohol dehydrogenases-likes from the MDR family (**Figure 1D**). Besides being collinear since they result from polyploidization (**Figure 1A and 1D**), these regions also shared a high degree of synteny with the locus enriched in genes encoding ADHs involved in heteroyohimbane synthesis (tetrahydroalstonine synthase, THAS)) found on chromosome 4 of *C. roseus* (**Sun et al., 2023**), suggesting a putative local duplication of *THAS1* and *THAS3* orthologs in *R. tetraphylla* prior WGT (**Supplementary Figure S5)**. We determined that 25 of the 28 genes were associated with a complete ADH protein clustering into 7 ADH identity groups (**Figure 1E**). A search for homology revealed that VR2 is located in the studied genomic regions and corresponds to Rte11bG086277, with two close homologs Rte11aG083588 and Rte11cG087148 (**Supplementary Table S7**). The three genes have a conserved local synteny (**Figure 1D**) together with a common phylogenetic clustering (**Figure 1E**).

Such a density in ADHs prompted us to investigate the activity of the genomic neighbors of VR2 that may encode the missing ADH of the ajmaline pathway. Based on a high expression level in roots (**Supplemental Figure 6**), one representative of each ADH identity group was thus amplified and assayed by transient expression in *Nicotiana benthamiana* together with VH and VR2 (**Figure 1F**; **Supplementary Methods**). While no modification in the feeded vinorine was observed in the control condition only expressing the green fluorescent protein (GFP) (**Supplementary Figure S7**), the overexpression of VH and VH combined to VR2 caused its conversion into vomilenine and 19,20-α(S)-dihydrovomilenine measurable at *m/z* 351 and 353, respectively (**Figure 1F**). These reactions fully agreed with the previously reported reaction catalyzed by VH and VR2 (**Dang et al., 2017**; **Geissler et al., 2016**). Outstandingly, the co-expression of Rte11bG086272 and Rte11cG087143 with VH and VR2 led to the formation of a new compound whose m/z (355) was consistent with an additional

reduction of 19,20-α(S)-dihydrovomilenine, potentially yielding 17-*O*-acetyl-norajmaline. In contrast, no similar reduction was observed while expressing Rte11cG087137, Rte11cG083572, Rte11cG087145 or Rte11bG086265 thus confirming the specificity of the reaction catalyzed by Rte11bG086272 and Rte11cG087143. It has to be noted that the individual co-expression of each of the four aforementioned genes with VH revealed that Rte11cG087145 catalyzed a vomilenine reduction similar to VR2 (**Supplementary Figure S8**).

To gain insight into the identity of the vomilenine derivatives produced through these assays, VR2, Rte11bG086272 and Rte11cG087143 were individually co-expressed with VH (**Figure 1G - left panel, Supplementary Figure S8**). As previously observed with VR2, we noted that Rte11bG086272 and Rte11cG087143 were capable of reducing vomilenine directly, as revealed by the formation of a *m/z* 353 product. However, the difference in the retention times of the VR2 and Rte11bG086272/Rte11cG087143 products strongly argue for the formation of two distinct compounds. We thus took advantage of these syntheses to assign the characteristic UV spectrum changes of vomilenine derivatives to the VR2 and Rte11bG086272/Rte11cG087143 products (**Figure 1H, Supplementary Figure S8**). As described by **Geissler et al. (2016)**, we first observed that both vomilenine and the VR2 product (19,20-α(S)-dihydrovomilenine) display similar spectra reaching two maxima at 221 nm and 269 nm. Interestingly, the Rte11bG086272/Rte11cG087143 product exhibits a radical spectrum shift with two maxima at 235 nm and 287 nm characteristic of the reduction of indolenine ring in 1,2-position found in 1,2-dihydrovomilenine. The identity of this compound was further confirmed by mass fragmentation that clearly revealed differences in the reduction catalyzed by Rte11bG086272/Rte11cG087143 and VR2 (**Supplementary Figure S9**). These results thus indicate that both Rte11bG086272 and Rte11cG087143 encode the missing enzyme of the ajmaline pathway catalyzing the 1,2 reduction of vomilenine, namely 1,2VR.

Lastly, to establish the preferential ADH reaction order, products generated by co-expressing VH and VR2 or VH and Rte11bG086272 or Rte11cG087143 (1,2VR) were further incubated for 24h with *N. benthamiana* disks expressing Rte11bG086272/Rte11cG087143 (1,2VR) and VR2, respectively (**Figure 1G - right panel ; Supplementary Figure S10**). Interestingly, we observed that the enzymes encoded by Rte11bG086272 or Rte11cG087143 (1,2VR) were not capable of reducing the VR2 product (19,20-α(S)-dihydrovomilenine) while VR2 efficiently reduced the Rte11bG086272 or Rte11cG087143 products (1,2-dihydrovomilenine). This strongly suggests that 1,2VRs (Rte11bG086272 or Rte11cG087143) catalyze the first vomilenine reduction followed by that catalyzed by VR2 in contrast to the previous hypothesis (**Geissler et al., 2016**).

In conclusion, this chromosome scale version of the *R. tetraphylla* genome provides valuable insights into MIA biogenesis through the identification of the missing enzyme of the ajmaline pathway. Outstandingly, VR2 and 1,2VR encoding genes were adjacent in the genome and also display a distant copy. Undoubtedly, this identification will pave the way for a future bioproduction of ajmaline in a heterologous organism.

FUNDINGS

This work was supported by EU Horizon 2020 research and innovation program [MIAMi project-Grant agreement N°814645]; ARD CVL Biopharmaceutical program of the Région Centre-Val de Loire [ETOPOCentre project]; and ANR [project MIACYC – ANR-20-CE43-0010].

Competing Interests

RP.D. and H.J.J are CEO and CTO of Future Genomics Technologies, respectively. M.K.J. has a financial interest in Biomia.

Author contributions

S.O.C., M.K.J., S.B. and V.C. jointly conceived and supervised the work. C.C., M.D., H.J.J., N.C., T.D.D.B., C.S. and R.P.D. performed chromosome counting, sequencing, assembly and genome annotation and analysis. E.L., I.C., V.V., C.B.W., A.O., J.P., N.P., performed enzyme characterization. E.L., C.C., M.D., S.B. and V.C. wrote the manuscript and designed the figures with input from all authors. All authors have read and approved the manuscript.

DATA AVAILABILITY

Raw DNA-seq data, Hi-C data, RNA-seq data and genome assembly have been deposited under the BioProject accession numbers: PRJNA771251 (https://www.ncbi.nlm.nih.gov/bioproject/PRJNA771251) and PRJNA1020772 (https://www.ncbi.nlm.nih.gov/bioproject/PRJNA1020772). The genome annotation, coding sequences, protein sequences and transcript sequences are available on the figshare: https://doi.org/10.6084/m9.figshare.21679628 (private link: https://figshare.com/s/3b080658774cf533f383).

GENE ACCESSION NUMBERS

Rte11cG087148 (OR571750); Rte11bG086272 (OR571751); Rte11cG087145 (OR571752); Rte11cG087143 (OR571753).

References

Dang TT, Franke J, Tatsis E, O'Connor SE (2017). Dual Catalytic Activity of a Cytochrome P450 Controls Bifurcation at a Metabolic Branch Point of Alkaloid Biosynthesis in Rauwolfia serpentina. *Angewandte Chemie (International ed. in English)*, *56*(32), 9440–9444. https://doi.org/10.1002/anie.201705010

Geissler M, Burghard M, Volk J, Staniek A, Warzecha H (2016). A novel cinnamyl alcohol dehydrogenase (CAD)-like reductase contributes to the structural diversity of monoterpenoid indole alkaloids in Rauvolfia. *Planta*, *243*(3), 813–824. https://doi.org/10.1007/s00425-015-2446-6

Kulagina N, Méteignier LV, Papon N, O'Connor SE, Courdavault V (2022). More than a Catharanthus plant: A multicellular and pluri-organelle alkaloid-producing factory. *Current opinion in plant biology*, *67*, 102200. https://doi.org/10.1016/j.pbi.2022.102200

Kumar S, Singh A, Bajpai V, Srivastava M, Singh BP, Ojha S, Kumar B (2016). Simultaneous determination of bioactive monoterpene indole alkaloids in ethanolic extract of seven Rauvolfia species using UHPLC with hybrid triple quadrupole linear ion trap mass spectrometry. Phytochemical Analysis, 27(5), 296-303. https://doi.org/10.1002/pca.2631

Kumar S, Singh A, Bajpai V, Srivastava M, Singh BP, Kumar B (2016). Structural characterization of monoterpene indole alkaloids in ethanolic extracts of Rauwolfia species by liquid chromatography with quadrupole time-of-flight mass spectrometry. Journal of pharmaceutical analysis, 6(6), 363-373. https://doi.org/10.1016/j.jpha.2016.04.008

Kumara PM, Shaanker RU, Pradeep T (2019). UPLC and ESI-MS analysis of metabolites of Rauvolfia tetraphylla L. and their spatial localization using desorption electrospray ionization (DESI) mass spectrometric imaging. Phytochemistry, 159, 20-29. https://doi.org/10.1016/j.phytochem.2018.11.009

Li, C., Wood, J.C., Vu, A.H., Hamilton JP, Rodriguez Lopez CE, Payne RME, Guerrero DAS, Gase K, Yomamoto K, Vaillancourt B, Caputi L, O'Connor SE, Buell CR (2023). Single-cell multi-omics in the medicinal plant Catharanthus roseus. Nat Chem Biol. https://doi.org/10.1038/s41589-023-01327-0

Sun, S., Shen, X., Li, Y., Li Y, Wang S, Li R, Zhang H, Shen G, Guo B, Wei J, Xu J, St-Pierre B, Chen S, Chao S (2023). Single-cell RNA sequencing provides a high-resolution roadmap for understanding the multicellular compartmentation of specialized metabolism. Nat. Plants 9, 179–190. https://doi.org/10.1038/s41477-022-01291-y

Zhang J, Hansen LG, Gudich O, Viehrig K, Lassen LMM, Schrübbers L, Adhikari KB, Rubaszka P, Carrasquer-Alvarez E, Chen L, D'Ambrosio V, Lehka B, Haidar AK, Nallapareddy S, Giannakou K, Laloux M, Arsovska D, Jørgensen MAK, Chan LJG, Kristensen M, Christensen HB, Suradarsan S, Stander EA, Baidoo E, Petzold CJ, Wulff T, O'Connor SE, Courdavault V, Jensen MJ, Keasling JD (2022). A microbial supply chain for production of the anti-cancer drug vinblastine. *Nature*, *609*(7926), 341–347. https://doi.org/10.1038/s41586-022-05157-3

FIGURE LEGEND

Figure 1. The chromosome scale genome of *R. tetraphylla* and identification of the 1,2-dihydrovomilenine reductase. (A) Genomic landscape of *R. tetraphylla*. Concentric rings present, from the outside to the inside: pseudo-chromosome name, pseudo-chromosome scale, gene density (purple: low density; yellow: high density) and transposable element density (blue: low density, brown: high density). Blue central links represent intra-chromosomal collinearity, light gray central links represent collinearity within a chromosome group and dark

gray central links collinearity between chromosome groups. (B) Synonymous substitution (Ks) rate distribution plot for *R. tetraphylla* (green) orthologs compared with *Catharanthus roseus* (blue) and *Vitis vinifera* (gray). WGT: whole genome triplication identified in *R. tetraphylla*, **γ**: conserved **γ** whole-genome triplication event that is shared among eudicots. (C) Phylogenetic tree of *R. tetraphylla* and eight other species including three Apocynaceae (purple: *C. roseus*, *V. minor*, *V. thouarsii*), one Gelsemiaceae (yellow: *G. sempervirens*), one Rubiaceae (green: *O. pumila*) and one Cornales (pink: *C. acuminata*). (D) Maps and synteny of the ADH enriched regions in chromosomes 11a, 11b and 11c. Only ADH genes are numerated, in black and in gray for complet and partial ADH sequences, respectively. Synteny between ADHs are highlighted with colors. (E) Neighbour joining phylogenetic tree (100 bootstrap replications) of predicted ADH protein sequences. Proteins in red were cloned and used for enzymatic assays. (F) Screening of ADH activities for reduction of 19,20-α(S)-dihydrovomilenine (VR2 product). ADH candidates were transiently expressed in tobacco leaves together with VH and VR2 in presence of vinorine and the reaction products analyzed by LC/MS. (G) Analyzes of the enzymatic order of VR2 and Rte11bG086272 after the vinorine hydroxylation by VH. Both ADH were, independently, transiently overexpressed in tobacco leaves with VH in presence of vinorine during 24h. The reaction medium of these two enzymatic assays were added, independently, with the other ADH during additional 24h and reaction products were analyzed by LC/MS. (H) UV spectra of vomilenine, 19,20-α(S)-dihydrovomilenine (VR2 product) and Rte11bG086272 product (1,2-dihydrovomilenine). (I) Preferential order of vomilenine reduction successively involving 1,2VR and VR2.

SUPPLEMENTAL DATA

Supplementary Methods.

Supplementary Table S1. Genome assembly metrics

Supplementary Table S2. Functional annotation of the predicted genes

Supplementary Table S3. Transposable element summary

Supplementary Table S4. Number of ADHs in *Rauvolfia tetraphylla*, *Catharanthus roseus* and *Vitis vinifera*.

Supplementary Table S5. Biosynthetic gene clusters identified by PlantiSMASH

Supplementary Table S6. Biosynthetic gene clusters identified using our personal script

Supplementary Table S7. Best-hit orthologs of MIA pathway genes in *Rauvolfia tetraphylla*

Supplementary Figure S1. *Rauvolfia tetraphylla* and its main MIA producing organs. (A) Overview of *R. tetraphylla* plant. (B) *R. tetraphylla* flowers. (C-D) *R.*

tetraphylla berries at different maturity stage. (E) *R. tetraphylla* triad leaves. (F) *R. tetraphylla* leaves. (G) *R. tetraphylla* roots.

Supplementary Figure S2. Proposed biosynthetic pathway of ajmaline. *SGD: strictosidine β-D-glucosidase, GS: geissoschizine synthase, SBE: Sarpagan bridge enzyme, PNAE: polyneuridine aldehyde esterase, VS: vinorine synthase, VH: vinorine hydroxylase, VR: vomilenine reductase, VR2: vomilenine reductase 2, DHVR: dihydrovomilenine reductase, AAE: acetylajmalan esterase, NAMT: norajmaline methyltransferase.*

Supplementary Figure S3. Genome characteristics of *R. tetraphylla*. (A) Contact map of Hi-C reads revealing the 33 chromosomes of *R. tetraphylla*. (B) chromosome counting.

Supplementary Figure S4. Comparative genomic analysis of *R. tetraphylla* and eight other plant species. Orthofinder phylogenetic tree of the nine studied species including four Apocynaceae (purple: *R. tetraphylla*, *C. roseus*, *V. minor*, *V. thouarsii*), one Gelsemiaceae (yellow: *G. sempervirens*), one Rubiaceae (green: *O. pumila*) and one Cornales (pink: *C. acuminata*). Orthogroup expansion (+) and contraction (-) was calculated using Cafe5. Light bordered boxes: expanded (+) or contracted (-) orthogroups in each lineage, Thick bordered boxes: expanded (+) or contracted (-) orthogroups in internal nodes of ancestral population for each taxon.

Supplementary Figure S5. Comparison between cluster-related ADHs of *R. tetraphylla* with *C. roseus* ADHs. (A) Synteny between *R. tetraphylla* clusters 352 (pseudo-chromosome 11a), 555 (pseudo-chromosome 11b), 567 (pseudo-chromosome 11c) and *C. roseus* ADH-rich region on pseudo-chromosome 4. The colored numbers indicate the position of ADH-encoding gene trios within the cluster. Colored boxes indicate orthogroups. ADHs and gene synteny blocks are indicated by colored and gray lines, respectively. (B) Neighbour-joining phylogenetic tree (100 bootstrap replications) of the cluster-related ADHs protein sequences of *R. tetraphylla* compared to THAS1, THAS2, THAS3, THAS4 and VR2. The colored numbers indicate the position of ADH-encoding gene trios within the cluster in (A).

Supplementary Figure S6. Expression profile of the cluster-related ADHs transcripts in several organs. The measured expression levels of the cluster related ADHs are displayed as transcripts per million in roots, seedlings, stems, leaves, young leaves, flowers and berries in a top to down arrangement. The boxplots were split according to phylogenetic tree analysis in Supplementary Figure S5B .Red arrows indicate cloned sequences used for enzymatic assays.

Supplementary Figure S7. Analysis of the VH enzymatic activity with vinorine to form vomilenine. VH and GFP were, independently, transiently overexpressed in tobacco leaves in presence of vinorine during 24h. VH reaction products were

analyzed by LC/MS as compared to a negative control (GFP) at m/z 335 (vinorine) and m/z 351 (vomilenine). *GFP: Green Fluorescent Protein. m/z: mass to charge ratio. VH: vinorine hydroxylase.*

Supplementary Figure S8. Screening of ADH activities for reduction of vomilenine (VH product). (A) Positive differential mass chromatograms of vomilenine reduction assays with ADH candidates (m/z 353) compared to GFP. ADH candidates and GFP control were transiently overexpressed in tobacco leaves with VH in presence of vinorine and reaction products were analyzed by LC/MS. (B) UV spectrum of the vomilenine (VH product, black line) compared to the reduced products of VR2 (Green), Rte11bG086272 (red), Rte11cG087143 (blue) and Rte11cG087145 (yellow). UV spectra were measured on peaks with an asterisk on panel A mass chromatograms. *m/z: mass to charge ratio. VH: vinorine hydroxylase. VR2: vomilenine reductase 2***.**

Supplementary Figure S9. Comparison of the MS/MS spectra of vomilenine reduced products (m/z 353). (A) The upper and lower panels contain respectively the reduced vomilenine (m/z 353) of VR2 and the reduced vomilenine of Rte11cG087145 spectrum, with a Pearson correlation score of 0.93. (B) The upper and lower panels contain respectively the reduced vomilenine (m/z 353) of Rte11cG087143 and the reduced vomilenine of Rte11bG086272 spectrum, with a Pearson correlation score of 0.99. (C) The upper and lower panels contain respectively the reduced vomilenine (m/z 353) of VR2 and the reduced vomilenine of Rte11bG086272 spectrum, with a Pearson correlation score of 0.67. Common peaks are drawn in a slightly darker colour for all three figures.

Supplementary Figure S10. Analyzes of the enzymatic order of VR2 and Rte11cG087143 after the vinorine hydroxylation by VH. Both ADHs were transiently overexpressed in tobacco leaves with VH in presence of vinorine during 24h. The reaction medium of these two enzymatic assays were added, independently, with the other ADH during additional 24h. Reaction products were analyzed by LC/MS.

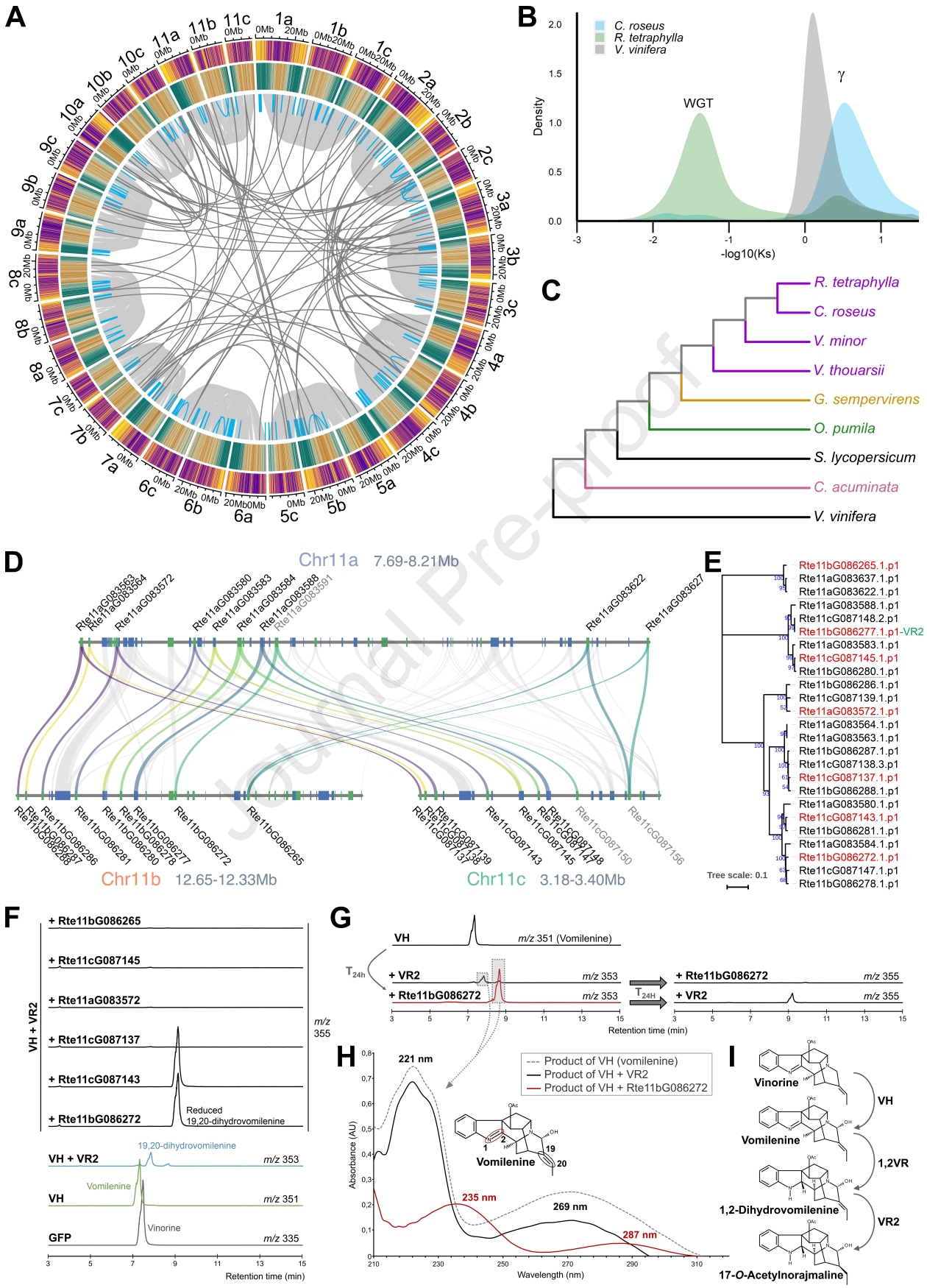
A
1a 1b 1c 2a 2b 2c 3a 3b 3c 4a 4b 4c 5a 5b 5c 6a 6b 6c 7a 7b 7c 8a 8b 8c 9a 9b 9c 10a 10b 10c 11a 11b 11c
B
C. roseus
R. tetraphylla
V. vinifera
WGT
γ
Density
-log10(Ks)
C
R. tetraphylla
C. roseus
V. minor
V. thouarsii
G. sempervirens
O. pumila
S. lycopersicum
C. acuminata
V. vinifera
D
Chr11a 7.69-8.21Mb
Chr11b 12.65-12.33Mb
Chr11c 3.18-3.40Mb
E
Tree scale: 0.1
F
+ Rte11bG086265
+ Rte11cG087145
+ Rte11aG083572
+ Rte11cG087137
+ Rte11cG087143
+ Rte11bG086272
Reduced 19,20-dihydrovomilenine
VH + VR2
m/z 355
19,20-dihydrovomilenine
m/z 353
Vomilenine
VH
m/z 351
Vinorine
GFP
m/z 335
Retention time (min)
G
VH
m/z 351 (Vomilenine)
T24h
+ VR2
m/z 353
+ Rte11bG086272
m/z 353
+ Rte11bG086272
m/z 355
+ VR2
m/z 355
Retention time (min)
H
221 nm
Product of VH (vomilenine)
Product of VH + VR2
Product of VH + Rte11bG086272
Vomilenine
235 nm
269 nm
287 nm
Absorbance (AU)
Wavelength (nm)
I
Vinorine
VH
Vomilenine
1,2VR
1,2-Dihydrovomilenine
VR2
17-O-Acetylnorajmaline

Competing Interests

RP.D. and H.J.J are CEO and CTO of Future Genomics Technologies, respectively. M.K.J. has a financial interest in Biomia.